Facilitated transport membranes containing graphene oxide-based nanoplatelets for CO_2 separation: Effect of 2D filler properties

Saravanan Janakiram [a], Juan Luis Martín Espejo [a], Xinyi Yu [a], Luca Ansaloni [b], Liyuan Deng [a],*

[a] Department of Chemical Engineering, Norwegian University of Science and Technology (NTNU), Trondheim, NO-7491, Norway
[b] Department of Sustainable Energy Technology, SINTEF Industry, 0373, Oslo, Norway

ARTICLE INFO

ABSTRACT

Realization of suitable membrane-based technology for efficient CO_2 capture to mitigate climate change relies on the development of thin-film composite (TFC) membranes with superior separation performance. Graphene oxide (GO), due to its 2D morphology, intrinsic strength and chemical compatibility, was used as a nanofiller to enhance CO_2 separation performance and stability of a facilitated transport membrane. SHPAA (sterically hindered polyallylamine)-based blend matrix was selected as the polymeric matrix material in this work. The high aspect ratio of GO-based fillers, when coupled with optimized coating protocol, resulted in TFC membranes of ultrathin (200 nm) selective layers with the in-plane orientation of nanoplatelets, leading to enhanced separation properties that can be retained for long term. Porous graphene oxide (pGO) was also incorporated as nanofillers, resulting in significantly improved gas permeation at a very low filler loading of 0.2 wt%; A CO_2 permeance of up to 607 GPU with a CO_2/N_2 separation factor of 36 in flat-sheet configuration was documented. Chemical modification of GO with PEG groups was found to further increase the selectivity of the membranes but reduces the CO_2 permeance, showing a CO_2/N_2 separation factor of 90 with a CO_2 permeance of 205 GPU. The effect of various 2D nanoplatelets on CO_2 transport properties in the membranes of hydrophilic PVA (polyvinyl alcohol) matrix and facilitated transport SHPAA/PVA matrix was elucidated with respect to the nanofiller property and loading.

1. Introduction

The global climate crisis is believed to be primarily due to industrialisation. Of all the causes, the tremendous increase in greenhouse gas emissions, most importantly, the emission of CO_2, over the past few decades, could be directly coupled to the current global warming scenario. Implementation of Carbon Capture, Utilization and Sequestration (CCUS) represents the most effective solution for the coming decade to undergo the transition to a more sustainable energy system. However, limitations relating to the cost and technical viability in the CO_2 capture technologies (i.e., absorption, membrane separation and adsorption) still pose as the main challenges to be addressed in the implementation of CCUS [1–3].

Polymeric gas separation membranes due to their low-cost, high modularity and easy scalability have been explored widely for CO_2 separation applications. Membrane materials with preeminent permeation properties (permeability and selectivity), as well as good chemical and mechanical properties, increase efficiency of separation processes

significantly [4–7]. Conventional polymeric membranes based on the solution-diffusion mechanism suffer due to the inherent trade-off between permeability and selectivity, as denoted by the Robeson upper bound [8]. Facilitated transport membrane is considered one of the successful approaches to overcome the trade-off and thereby improve separation performance, which uses CO_2-reactive carriers to enhance CO_2 transport. Another approach is to make hybrid membranes to combine the advantages of inorganic materials, including the use of nano-sized fillers to make nanocomposite membranes, which also synergistically exploit properties arising at the nanoscale [9–12]. However, limited studies have reported the combination of these two approaches to increase water uptake of facilitated transport membranes by taking advantages of the hydrophilicity of the added filler phase and to enhance the mechanical stability of the fully swollen membrane matrix except for a few reports [13–15]. Nevertheless, the incorporation of 2 dimensional (2D) nanoplatelets in facilitated transport membranes has rarely been reported in the form of ultrathin selective layers less than 500 nm suitable for application in CO_2 separation. The fabrication of the TFC

---

* Corresponding author.
  E-mail address: liyuan.deng@ntnu.no (L. Deng).

membrane with such ultrathin selective layers comprising of 2D nano-platelets in facilitated transport membranes using a scalable fabrication procedure seems challenging.

Due to their large aspect ratio, 2D materials such as graphene oxide (GO) significantly influence mechanical and transport properties when added as nanofillers in hybrid membranes. GO is inherently a barrier for gas permeation, but it can be engineered to benefit the gas permeation in a membrane. With a large surface-to-volume ratio, nanoplatelets of GO inherit high mechanical strength. The presence of hydroxyl groups on the GO surface also brings in hydrophilicity and increased surface interaction with CO_2 [16–18]. On the other hand, the barrier properties of GO platelets can be significant even at low loadings in hybrid matrices depending on the physical and chemical properties of the 2D nanoplatelets.

In general, the challenges using 2D fillers include incompatibility between filler and polymer, upscaling complexity to form defect-free thin composite membranes, and morphology/chemical property tuning of fillers [10]. Dong et al. [19] added GO nanoplatelets to hyper-branched polyethyleneimine (HPEI) and trimesoyl chloride (TMC), and fabricated composite membrane with the highest permeance of 9.7 GPU and CO_2/N_2 selectivity of 80. Shen et al. [20] fabricated PVAm and Chitosan based hybrid membrane with HPEI modified GO enhancing the CO_2 permeance from 14 GPU to a maximum of 36 GPU and a maximum CO_2/N_2 selectivity of 107 from 80. A few other studies explore the use of GO platelets in membranes for CO_2 separation, but most studies are based on thick self-standing films [21–23]. Recently, Wang et al. [24] reported a PVAm-based GO/CNT mixed matrix composite membrane with a maximum CO_2 permeance of 275 GPU and CO_2/N_2 selectivity of 155.1 by tuning the interlayer spacing with the addition of CNTs as a third component.

In this work, we incorporated a very small amount of GO-based 2D nanoplatelets into facilitated transport membranes (~0.2% loading) to improve the CO_2 permeation performance and their long-term stability in the humid environment. Ultrathin, defect-free selective layers (~200 nm) containing 2D nanosheets were coated on porous flat sheet supports using a scalable, facile method. Both physically and chemically modified GO platelets with an array of properties were synthesized or modified for the successful dispersion of these 2D nanofillers in the polymeric matrices of the ultrathin membranes (e.g., polyvinyl alcohol (PVA) and the blend of sterically hindered polyallyl amine (SHPAA) with PVA). The nanofillers and hybrid membranes were thoroughly characterized, and the separation performances of the developed membrane was systematically assessed by both single gas and mixed gas permeation tests under humid conditions. The effects of the nanofillers on the improvement of the membrane morphologic and separation performance were analysed.

2. Materials and methods

2.1. Materials

Poly(allylamine hydrochloride) (Mw = 120,000–200,000) was purchased from Thermo Fisher Scientific, Sweden, and was purified and modified into sterically hindered polyallylamine.

SP1 grade synthetic graphite powder from Bay Carbon Inc., USA, was used as received. Sulphuric acid (97%), hydrochloric acid (35%) and acetone (99.5%) used in GO synthesis were purchased from Daejung Chemicals & Metals Co., South Korea. Hydrogen peroxide (50% in water) and potassium permanganate used in synthesis and modification of GO were supplied by Junsei Chemical Co., Japan.

Potassium hydroxide (pellets, 85%–100%), polyvinyl alcohol (Mw = 89,000–98,000, 89% hydrolyzed), 1-Ethyl-3-(3-dimethylaminopropyl) carbodiimide, N-hydroxysulfosuccinimide, 2-bromopropane, Methanol (anhydrous, >99.8), 8arm-poly (ethylene glycol)-NH$_2$ (hexaglycerol core, Mn = 10,000, PEG), were used as received from Sigma-Aldrich, Norway. Polyvinylidene fluoride (PVDF) ultrafiltration membrane (50

k MW) with polypropylene (PP) substrate was obtained from Synder Filtration, USA. 3 M™ Fluorinert™ Electronic Liquid FC-72 was used as received from Kemi-Intressen, Sweden. CO_2/N_2 mixture (10 vol% CO_2 in N_2) and CH_4 (99.95%), used for permeation tests, were supplied by AGA, Norway. Hydrogen peroxide (H_2O_2, 30% in water) used in the modification of GO was supplied by Sigma Aldrich, Norway.

2.1.1. Synthesis of sterically hindered polyallyamine (SHPAA)

Sterically hindered polyallylamine was obtained by modification of purified polyallylamine with 2-bromopropane, as reported in our previous work [13]. Poly allylamine reacts with 2-bromopropane in the presence of stoichiometric amounts of KOH at 50 °C under reflux conditions in methanol yields poly-N-isopropyl allylamine [25], as shown in reaction Scheme 1.

### 2.1.2. Synthesis of graphene oxide and its modification

Graphene oxide used in the flat sheet membranes was synthesized through modified Hummer's method, as reported in Ref. [26,27]. 10 g of graphite powder was mixed with 450 mL of Sulphuric acid under stirring at 5 °C for 1 h. 30 g of potassium permanganate was then added and stirred for 30 min, resulting in a colour change from black to dark green. The solution was further heated up to 40 °C for 1 h. 450 mL of deionized water was added dropwise and carefully to avoid a rapid increase in temperature. The solution is characterized by a colour change to dark brown at this point. The temperature was then maintained at 95 °C for 30 min followed by adding 300 mL of 10% hydrogen peroxide solution and then stirred for 15 min. The colour change to light brown marked the successful synthesis of graphene oxide. The GO was then purified multiple times with about 5 L of 10% hydrochloric acid through a Whatman glass microfiber filter followed by washing in 3 L of acetone. The filtered GO cakes were then dried at 40 °C for two days under vacuum. Prior to usage, GO flakes are dispersed in the required quantity of water and sonicated with a tip sonicator for 3 h for exfoliation.

2.1.3. Physical modification of graphene oxide

In order to physically modify GO flakes for better diffusion of penetrants, random pores were introduced by hydrothermal treatment of GO using hydrogen peroxide, as reported earlier by Lee et al. [27]. 1 M NaOH was used to adjust pH of 75 mL of 1 mg mL^{-1} GO solution was taken and the pH was adjusted to 10 using 1 M NaOH solution. The mixture was stirred for 5 min at high speed followed by bath sonication for 10 min 10 mL of 3% dilute hydrogen peroxide solution was then added to the mixture and the solution was stirred for 10 min at high speed followed by bath sonication for 10 min. The resulting mixture was then treated at 180 °C in a Teflon autoclave for 6 h and then cooled down to room temperature. The resulting pGO dispersion in the water had a concentration of about 1 mg mL^{-1}.

2.1.4. Chemical modification of graphene oxide

PEG groups were grafted onto the GO surface using the EDC coupling reaction [13,28]. GO basal planes are characterized with acidic –COOH edge groups. However, in order to activate multiple sites for PEG grafting for amide bond formation, further carboxylic groups on GO surface were introduced by treating 20 mL of 4 mg mL^{-1} GO dispersion with an equal volume of 3 M NaOH followed by bath sonication for 1 h at 25 °C. This reaction enabled the conversion of esters in GO surface to be hydrolyzed into carboxylic groups in addition to the edge carboxylic
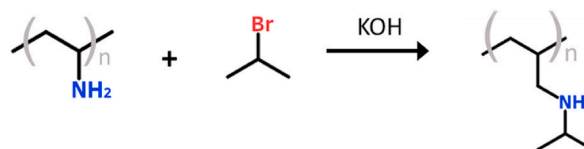
Scheme 1. Steric hindrance of polyallylamine.

groups already present in the GO. Dilute HCl was then added to neutralize the solution followed by dilution to 1 mg mL^{-1}, obtaining a dispersion of carboxylated GO in water. 100 mg of NHS and 150 mg of EDC was then added to the GO-COOH dispersion, followed by bath sonication in ice for 30 min to activate the catalysts. 200 mg of 8-arm PEG was then added to the mixture, and the solution was stirred at room temperature for 24 h. The solution was then centrifuged at 7000 rpm to remove aggregates, and the dispersion was then dialyzed in water using Dialysis membrane Spectra/Por® 3 to remove the catalysts, salts and other unreacted components. The residual dispersion had a GO-PEG concentration of about 1 mg mL^{-1}.

2.1.5. Coating of composite membranes

4 wt% PVA solution in water was prepared by dissolving PVA pellets in deionized water at 80 °C for 4 h under reflux conditions. The SHPAA solution in methanol post-modification was dried at 60 °C under vacuum overnight to remove residual solvent. The resulting pristine polymer was then dissolved in water for 24 h in room temperature to obtain a 6 wt% solution.

In the case of flat sheet membranes, a cast solution concentration of about 1 wt% was used. The blend polymer solution of SHPAA/PVA constituted 90 wt% SHPAA and 10 wt% PVA of the total polymeric solids present in the solution. The % amount of nanofillers was measured with respect to the total polymer present in the cast solutions. For example, a 0.5 wt % GO in SHPAA/PVA blend denotes that the amount of GO is 0.5% of the total polymer present in the solution. The PVDF support was first washed in tap water at 45 °C for 1 h followed by DI water for 30 min to remove the pore protective agent. The support was dried at room temperature overnight prior to coating using a bar coating machine as described in our previous work. Low-boiling FC-72 was used to fill the pores to avoid pore penetration of the casting solution.

2.2. Material and membrane characterization

Chemical changes to nanofillers were monitored by Fourier-transform infrared (FTIR) spectroscopy using Thermo Nicolet Nexus spectrometer equipped with smart endurance reflection cell in attenuated total reflectance mode with a diamond crystal. An average of 16 scans with a resolution of 4 cm^{-1} was used in the range of 4000 cm^{-1} and 800 cm^{-1} to build the spectra. The surface chemical composition of synthesized GO was analysed with an X-ray photoelectron spectroscopy (XPS, XPS-theta probe, Thermo Fisher Scientific Co., USA) equipped with a monochromatic Al Kα source with C-correction of 284.5 eV.

Membrane morphologies were analysed by Field Emission SEM APREO (FEI, Thermo Fisher Scientific, USA) equipped with an in-lens detector under immersion mode. Before analysis, the samples were sputter-coated with 8 nm Pd/Pt alloy.

The synthesized nanofillers were observed for structural details using Hitachi S-5500 S(T)EM (Hitachi High Technologies America, Inc.). Both bright field and dark field detectors were used for transmission measurements. The samples were prepared by dispersing a drop of dilute filler suspensions on 300 mesh Cu grids (Electron Microscopy Sciences, FCF300–Cu). EDX analysis was performed with Bruker EDX-system (Bruker XFlash EDX Detector) for elemental mapping.

Atomic Force Microscope (AFM) (AFM Dimension Icon, Bruker, USA) was used to study the alignment of GO in bar-coated samples. The imaging was done in ScanAsyst QNM tapping mode using a silicon nitride tip. The samples were prepared by bar coating casting solutions or by drying a drop of casting solution on freshly cleaved mica sheets followed by drying at 60 °C.

2.3. Gas permeation performance

The gas permeation performance of the fabricated membranes was evaluated by a humid gas permeation rig, as reported in our previous studies [13,29,30]. A constant flow of 10/90 v/v CO_2/N_2 mixture of 200

mL min^{-1} was used as a feed in order to maintain a low stage cut (less than 0.5%). The feed pressure was maintained at 1.7–2 bar. CH_4 was used as a sweep gas at a volumetric flow rate of 100–200 mL min^{-1} at a pressure of around 1.02 bar. Both feed and sweep streams were humidified in a bubble tank prior to contact over the active membrane surface. Steady-state compositions of the permeate, retentate and the feed streams were monitored in line regularly using pre-calibrated gas chromatography (490 Micro GC, Agilent). The permeance of the gas component '*i*' was obtained using the following equation:

$$P_i = \frac{2 \cdot \dot{n}_p \left(1 - y_{H_2O}\right) y_i}{\left(\left(p_{i,f} + p_{i,r}\right) - 2 \cdot p_{i,p}\right) A} \tag{1}$$

Where $\dot{n}_p$ is the total permeate flow in cm^3(STP) s^{-1} measured at the exit with a bubble flow meter after reaching the steady state. y_{H_2O} and y_i denote the molar fraction of the water and permeating species in the permeate flow, respectively. $p_{i,f}$, $p_{i,r}$ and $p_{i,p}$ are the partial pressures in cmHg^{-1} of the species '*i*' in the feed, retentate and permeate, respectively. A is the effective permeation area in cm^2. In this study the permeance is reported in GPU, where 1 GPU $= 10^{-6}$ cm^3(STP) cm^{-2} s^{-1} cmHg$^{-1} = 3.35 \times 10^{-10}$ mol m^{-2} s^{-1} Pa^{-1}. Additionally, the separation factor was calculated according to Equation (2):

$$\alpha_{i/j} = \frac{y_i/x_i}{y_j/x_j} \tag{2}$$

where *y* and *x* represent the molar gas concentration in the permeate and feed stream, respectively. For pure gas humid permeation tests, the feed gas was switched to pure gas with an upstream pressure of 1.1 bar. Similar conditions were used in the sweep side. The CO_2/N_2 ideal selectivity was calculated as the ratio between CO_2 and N_2 pure gas permeances.

3. Results and discussion

3.1. Synthesis and modification of fillers

The successful synthesis of GO is confirmed by the characterization of the nanoplatelets with the X-ray photoelectron spectroscopy. Baseline subtraction was done by the Shirley approach, and the C1s spectra were decomposed and fit using Gaussian and Lorentzian line shapes [31,32]. The corresponding spectra for both GO and pGO are seen in Fig. 1. Both GO and physically modified pGO are characterized by significant peaks that originate from C–C at ~285 eV and from C–O at ~287 eV. Additionally, small amounts of C=O groups are also evident in both the samples with a peak at ~288.5 eV. During the synthesis of GO, as a result of increasing oxidation, sp^2 carbon bonds of graphite functionalize into sp^3 and additionally to other oxygen containing groups such as hydroxyl, carboxyl and epoxy groups, as seen in Fig. 1A [33]. Likewise, for pGO, peroxide treatment to generate pores in GO led to the redistribution of peak intensity further in favour of C–O from C–C, as shown in Fig. 1B. This supplementary oxidation effect prompted by the modification procedure employed to make the porous GO is also confirmed by the reduced C/O ratio determined by XPS, where the pGO had a slightly lower ratio of 1.74 as opposed to that of GO at 1.79. Similar reduction in C/O ratio was reported by Lee et al. [27].

Morphological analysis of the synthesized and modified nanoplatelets was studied using S(T)EM. The representative results for GO and pGO are presented in Fig. 2. The high aspect ratio of GO nanoplatelets was evident from the sheet-like morphology with varying transparency typical of few-layered GO [34]. Folded structure of GO flakes [35] with two lateral dimensions in the order of microns were observed, corroborating the presence of stacked monolayers. On the other hand, discernible pores were observed in the order of nanometers on the pGO samples. It should be noted that these pores were not engineered to a particular pore size distribution for the sieving effect.
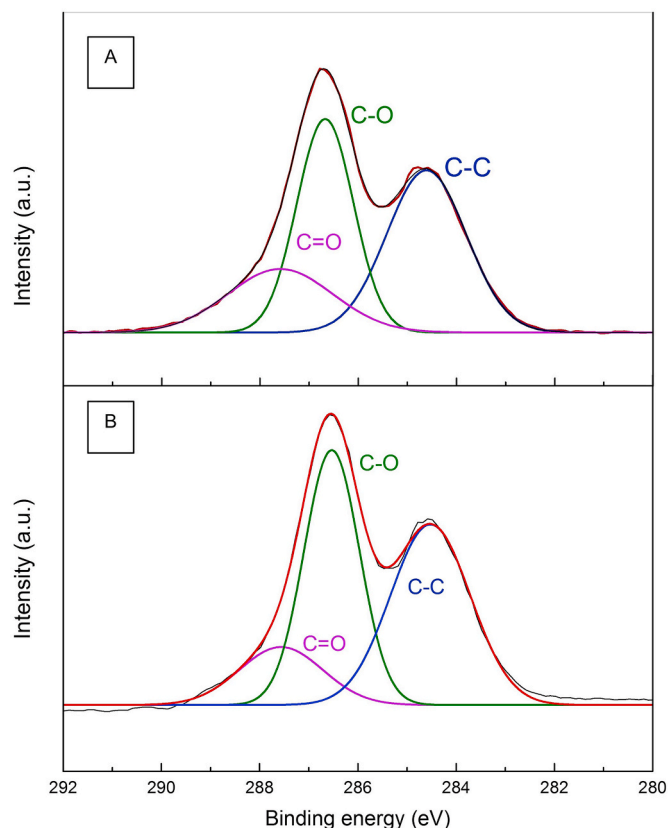
Fig. 1. Deconvoluted C 1s XPS spectra of synthesized (A) GO and (B) pGO.

The physical modification, which was used, is expected to create defects in the plane perpendicular to the direction of gas transport while preserving the 2D morphology of the original platelet. Fig. 2 confirms the presence of porous 2D platelets in pGO with the lateral dimensions considerably reduced when compared to GO nanoplatelets, which can be attributed to the fracture of GO during the hydrothermal treatment at weaker sp^3 regions [36]. In an attempt to characterize the pores, N_2 physisorption tests were also performed as described in the Supplementary Information (Figure S1).

Additionally, the chemically modified GO with PEG-grafted surfaces were examined with S(T)EM-EDX analysis to study the chemical composition on the surface. As the PEG groups were grafted at specific functional sites in the GO through the amide linkage, EDX analysis was performed to see the distribution of PEG groups that are end terminated with amine linkages. According to Fig. 3, the physical morphology of the GO-PEG nanoplatelets remained similar to the GO. As seen in the corresponding EDX maps, there exists a spatial distribution of N which originates from the PEG functionalization, due to amide group formation (dehydration reaction) and the terminal amine groups in the free arms of PEG (pristine GO basal planes do not feature N-containing groups). Elemental mapping of C and O are indicative of both C–O groups in the basal plane of GO and that of the PEG groups which are attached to the GO surface. It should be noted that the marked contrast differences in the SEM imaging arise due to the folded structure of the flakes [37] and hence high concentrations of individual elements in the corresponding EDS mapping are indicative of presence of a GO layer underneath.

Chemical changes due to the modification procedure were monitored by FTIR spectroscopy of the nanofillers in dispersion mode ($\sim$1 mg mL^{-1} solids in water). The spectra of the fillers are shown in Fig. 4. Peaks associated with free –OH groups due to the large amounts of water in the dispersion represent the broad band corresponding to the frequency range of 2750–3500 cm^{-1} and a sharp peak at 1640 cm^{-1}. Typical peaks associated with GO include 1097 cm^{-1} for -C-O-C stretching, 1412 cm^{-1} for –OH bending vibrations; -C-O- stretching at 1218 cm^{-1} and 1730 cm^{-1} for stretching of –C=O bonds with its associated -O-H stretching and bending at 1400 cm^{-1} [38,39]. With carboxylation, in GO-COOH, the intensity of –C=O increases relative to other peaks as expected due to the formation of new carboxyl groups. The spectra of pGO remained similar to that of GO except for considerable peak intensity reduction of -C-O-C stretching but more pronounced -C-OH stretching shoulder at 1218 cm^{-1}. This could be attributed to partial oxidation of most epoxy groups to respective hydroxyl groups by the ȮH from the peroxide [40]. In the case of GO-PEG, the functionalization of PEG groups to GO surface is confirmed by the formation of amide bond with an obvious NH deformation peak at 1530 cm^{-1} denoting and corresponding C=O stretching associated with secondary amine groups at 1643 cm^{-1} [13,41]. Also, PEG functional groups are characterized with -C-H stretching at 1453 cm^{-1} and C–H bending vibrations at 1342 cm^{-1}. Additionally, with functionalization, there exists a peak shift of -C-O-C stretching to the left, which is representative of PEG groups than epoxy groups in the basal plane of GO.
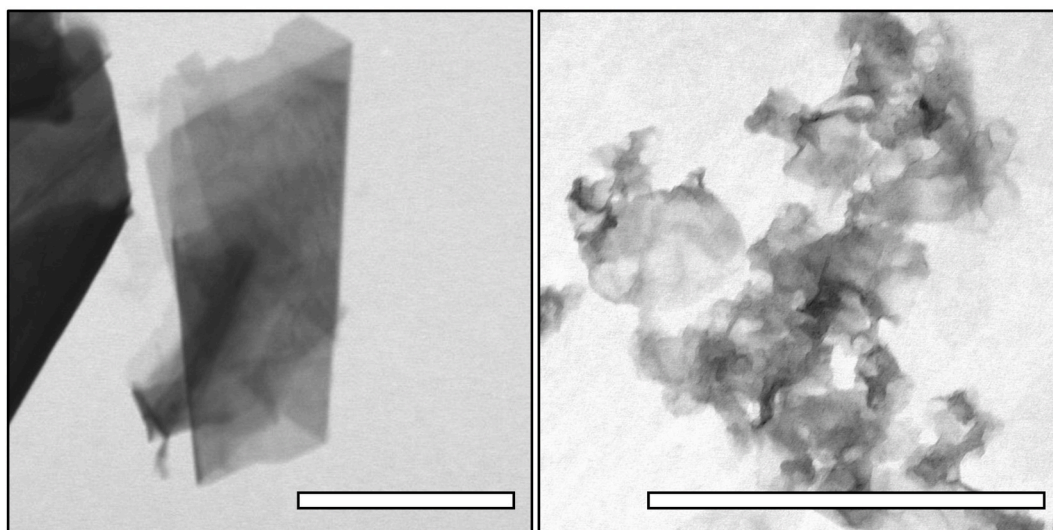

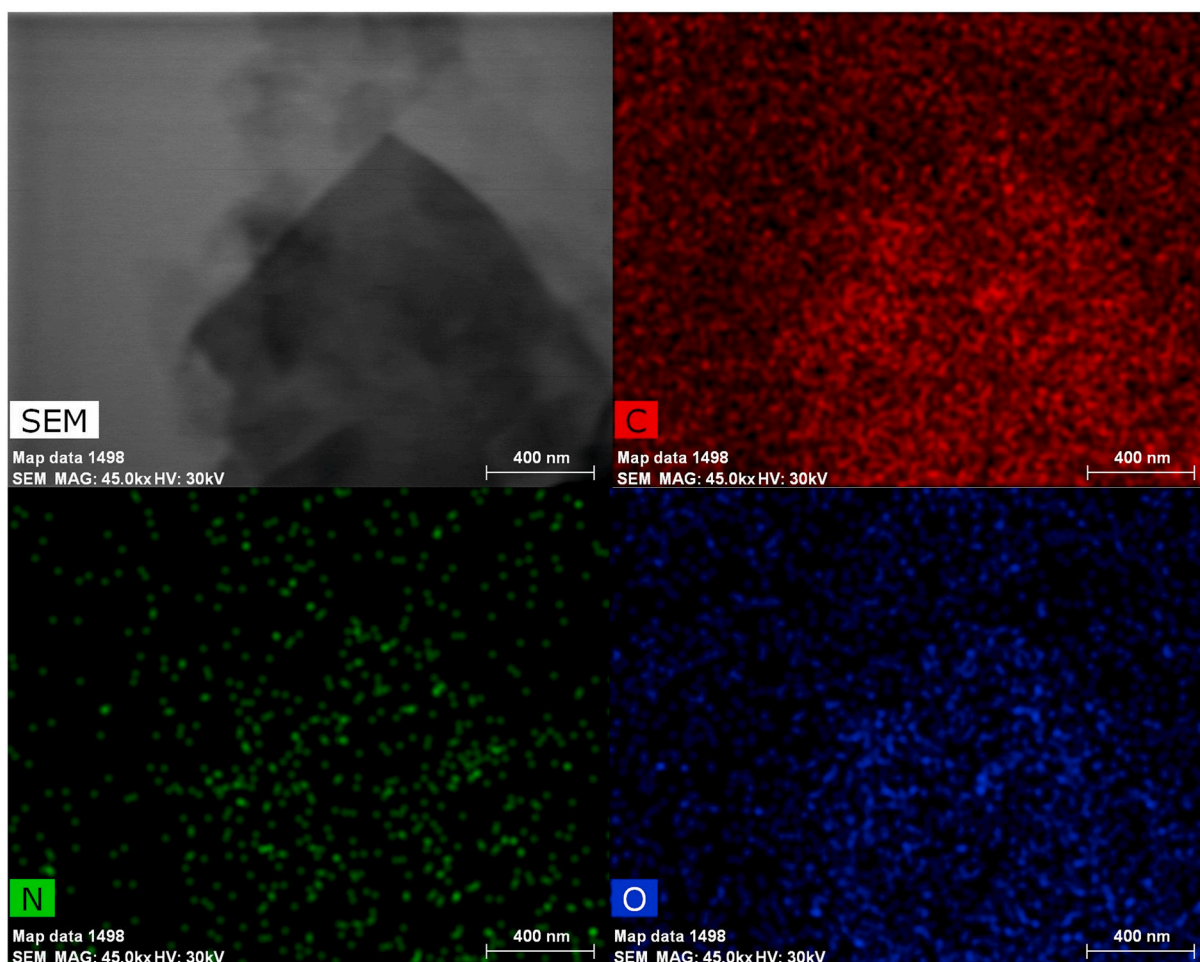**Fig. 2.** S(T)EM imaging of GO (left) and pGO (right) (Scale bar = 500 nm).

Fig. 3. S(T)EM image (top left) of GO-PEG with the elemental mapping of C (top right), N (bottom left) and O (bottom right).

3.2. Characterization of thin membranes with GO-based fillers

Stable dispersion of GO-based fillers with both PVA and SHPAA/PVA blend matrices was obtained at the entire range of filler loading from 0.2 wt% to 1 wt%. The concentration of cast solutions was maintained at 1 wt% of solid, much lower than the amount in the literature previously reported on GO dispersibility in PAA solutions for other applications [42]. The low concentration of polymer along with the reduced reactivity of amines to epoxy groups on the GO-based fillers caused by steric hindrance have led to a stable homogeneous polymer-filler dispersion with no visible agglomeration. The similar viscosities of coating solutions and the low density of GO flakes enabled similar coating layer thicknesses in all the fabricated hybrid membranes regardless of the 2D filler types and loadings. Representative cross-sectional SEM imaging of 0.2 wt% pGO loaded composite membrane, as seen in Fig. 5, reveals the presence of an ultrathin selective layer with a thickness lower than 200 nm on the PVDF porous support. Contrarily, the surface images of the selective layers show visible difference between the neat polymer membranes and those loaded with 2D nanofillers (Fig. 6). While neat polymer membrane showed an even surface, dark patches were observed in the hybrid membrane samples, which could be associated with the parallelly oriented GO-based filler flakes with incircle radii of less than 1 μm from the top view. No evident protrusion or aggregation of the nanofillers were observed from the smooth surface. Monolayer GO nanoplatelets are characterized with thickness about 1 nm with lateral dimensions ranging up to a micron as seen in Fig. 2. The smooth surface of the hybrid matrices of both GO and pGO loaded membranes with discernible spots yet no protrusions across a 200 nm thin selective layer

confirm the in-plane orientation. Such in-plane orientations have been reported due to the surface energy changes and reciprocal shear caused by the coating methods like dip-coating [43] or spin-coating [44]. These orientations depend on compatibility of GO nanoplatelets with the dispersed polymeric host matrix and method of preparation. Longer evaporation times by solvent evaporation method with thicker selective layer might result subsequent reduction of free energies unless externally controlled. In this study, the selective layer is coated by the bar-coating method, and the in-plane orientation of GO is attributed to the lowering of surface free energies of GO-based fillers [45] by mechanically forced-orientation of the thin 2D flakes into the tangent to the cylindrical surface of the bar at the contact point, as schematically represented in Fig. 7. This phenomenon along with the fast evaporation rate due to the coating of an ultrathin layer leads to the in-plane orientation of 2D fillers. Alternatively, PVA films containing GO nanoflakes were also prepared by solvent-evaporation method as a comparison, as seen in Fig. S2. These films show no visible patterns on surface SEM (Fig. S3) due to the random orientation of platelets, which can be attributed to longer evaporation times and the absence of an external force that orients the nanosheets.

The AFM analysis was also carried out to further study the orientation of GO in the bar-coated thin layer. Cast solutions of neat PVA polymer and PVA containing 0.2 wt% GO were used for this study. Similar coating procedure employed in membrane fabrication was used and the selective layer was bar-coated directly on to a freshly cleaved mica surface. Figs. 8.1A and 1B show the AFM images of a neat polymer layer. A topology indicating mild roughness was observed with the neat polymer sample. Interestingly, the sample containing PVA with 0.2 wt%
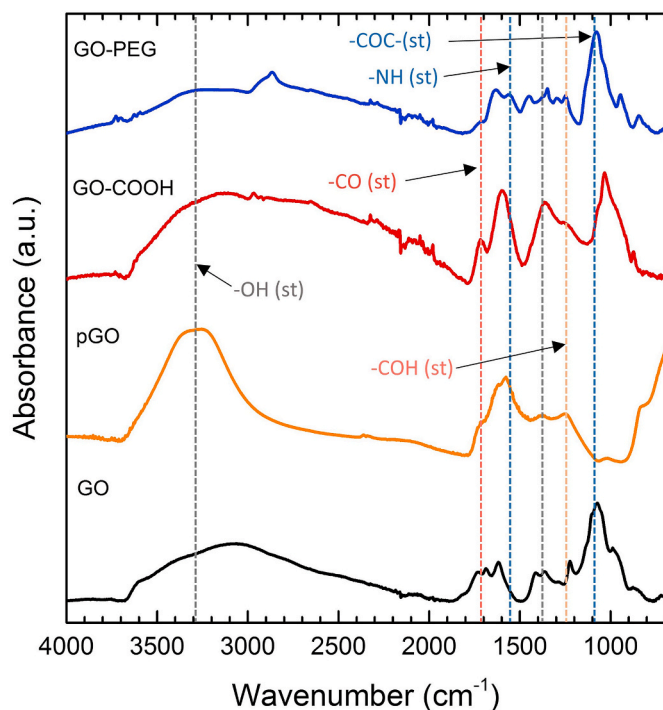
Fig. 4. FTIR spectra acquired from dispersions of GO, pGO, GO-COOH and GO-PEG (labelled and colour-coded). (For interpretation of the references to colour in this figure legend, the reader is referred to the Web version of this article.)

GO inherited the qualities of the neat PVA film but with additional characteristics indicating the presence of GO monolayers under the thin polymeric layer. The relatively lower roughness patterns in Fig. 8.2B than that in 8.1 B implies wrapping of PVA chains around GO due to their good compatibility. The overall height of the specimens are also similar, confirming the in-plane alignment of GO nanoflakes. This alignment was not achieved when drops of PVA containing 0.2 wt% GO was directly dried over mica support without using bar-coater as seen in Fig. S4. The roughness in the solvent evaporated specimen remained high due to the random orientation of GO nanoflakes when compared to the bar-coated counterpart, thus proving the effectiveness of the adopted method to align the nanoflakes in-plane with the coating surface.
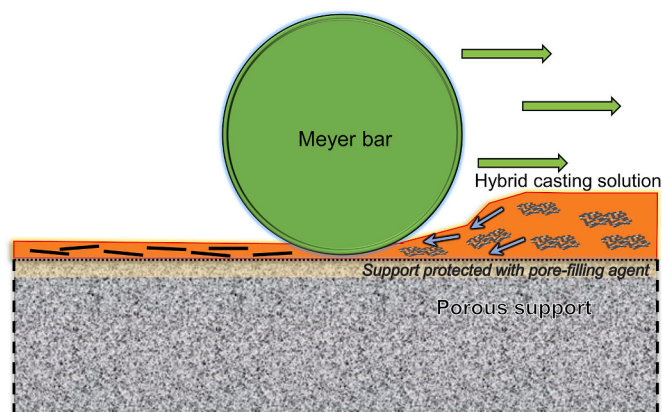

Fig. 7. Schematic illustration of orientation of GO-based fillers in hybrid membranes fabricated using bar coating technique.
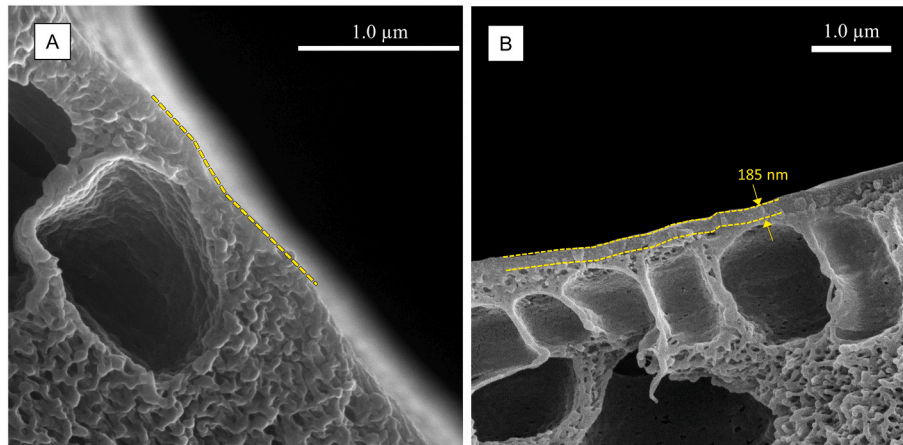

Fig. 5. Cross-section SEM images of (A) porous PVDF support (B) composite membrane containing SHPAA/PVA with 0.2 wt% pGO.
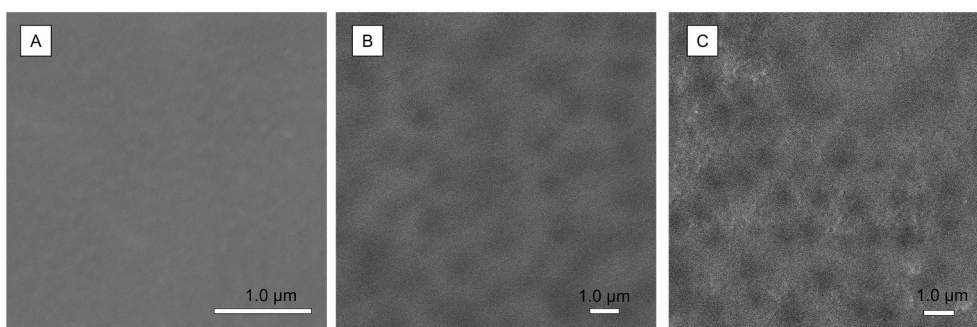

Fig. 6. Surface SEM images of membranes with (A) neat SHPAA/PVA (B) SHPAA/PVA with 0.2 wt% GO (C) SHPAA/PVA with 0.2 wt% pGO.
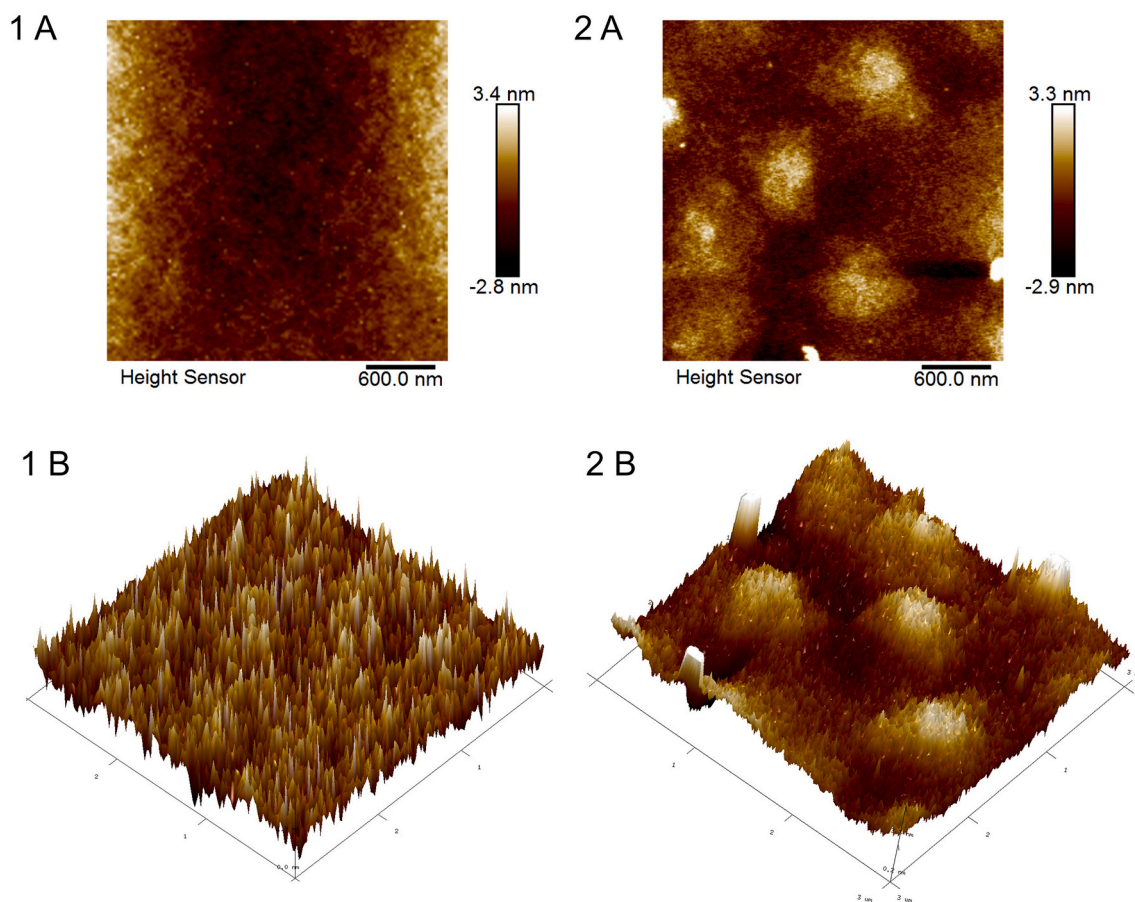
Fig. 8. AFM images of height in 2D (A) and 3D (B) from bar coated samples of (1) neat PVA cast solution and (2) PVA with 0.2 wt% GO.

3.3. Gas permeation performance

3.3.1. Hybrid membranes with PVA polymer matrix

Gas permeation performance of the fabricated membranes was analysed using a mixed gas permeation test rig with a humid feed mixture containing 10/90 v/v CO_2/N_2 at 35 °C. The results for PVA membranes loaded with GO-based fillers are shown in Fig. 9. PVA, although not a facilitated transport matrix, was chosen to distinguish the effects of GO-based fillers in water-swelling polymer matrix from fixed-site facilitated transport polymer (SHPAA). As it can be seen, the addition of GO influences the gas separation performance differently.

GO nanoflakes are characterized by their prominent gas barrier properties due to the strong π-orbital interactions, leading to the dense packing of aromatic rings in the basal plane [46,47]. This repulsive behaviour to gas permeation was notably observed in membranes of PVA with both GO and pGO fillers, where the CO_2 permeance of neat PVA drops from 240 GPU to ~140 GPU in the case of 0.2 wt% GO and to ~185 GPU in the case of pGO. Interestingly, the CO_2/N_2 selectivity did not increase as expected, but remained nearly constant [48]. On the other hand, with the addition of PEG modified GO into the PVA membrane, a notable increase in CO_2 permeance (to ~285 GPU) and a marginal increase in selectivity to ~49 were observed. Pure gas tests were also conducted in these membranes where a minor increase in performance with respect to CO_2 permeance was observed due to elevated CO_2 partial pressure in the feed. Addition of GO-based nanoplatelets was aimed increasing CO_2-philicity of the PVA matrix, however, their 2D structure imparts the barrier effect to gas permeation in the matrix. This barrier effect is well-pronounced with addition of GO-nanosheets in PVA, while with pGO containing less diffusion resistance, the effect rescinds gradually. With addition of GO-PEG, the EO groups add to enhanced CO_2 sorption along with good compatibility
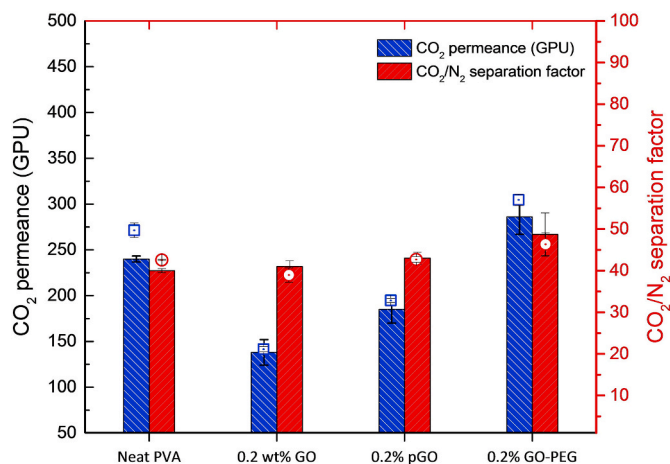

Fig. 9. Mixed gas permeation performance of various PVA-based hybrid membranes measured at 35 °C. (Symbols denote corresponding pure gas permeation data). Hybrid membranes with facilitated transport SHPAA polymer matrix.

with the hydroxyl groups of PVA matrix. The corresponding synergetic effect of PEG moieties blending with PVA has led to a positive effect on the separation properties [49].

Facilitated transport membranes transport CO_2 through a reactive pathway in addition to the solution-diffusion mechanism [50,51], which usually brings in both higher CO_2 permeation and selectivity of CO_2 over other more inert gases. In this work, the facilitated transport effect is brought in by the amine groups attached to the main chain of the

backbone in the SHPAA polymer matrix, which reversibly react with CO_2 in the presence of water [13]. With these enhanced CO_2 permeation pathways, the separation performance of neat SHPAA/PVA blend membrane was marked at the CO_2 permeance of 383 GPU (60% higher than that of PVA) and a CO_2/N_2 separation factor of 55, as shown in Fig. 10.

The GO platelets are able to induce the reorientation of chain packings when dispersed in polymers [48,52] due to their large surface-to-volume ratio in tandem with their 2D morphology. In the case of a facilitated transport polymer matrix, the reduced crystallinity due to coercive packing disruption enables faster diffusion and increases sorption of CO_2 by its enhanced access to the amine groups in the polymer backbone. The high surface area of the dispersed GO-nanosheets leads to increased active CO_2 sorption along the surface, supplementing the CO_2 solubility in the amine-containing polymer matrix. Additionally, the nanoplatelets are also expected to redistribute water domains present in the humidified matrix due to the vast spatial distribution arising from their large surface-to-volume ratio [16,53]. As water plays a significant role in CO_2 facilitated transport, the availability of water-rich domains distributed throughout the hybrid membrane is critical to ensure the enhanced CO_2 permeation across the membrane by the efficient absorption in the feed side, fast diffusion through the water swollen matrix, and desorption of CO_2 in the downstream side of the membrane [14,54,55]. Furthermore, the inherent mechanical strength of GO platelets contributes positively to the mechanical properties of the fully water swollen membranes at humidified conditions [14,15].

The separation performance of SHPAA/PVA membranes with different GO-based fillers are summarised in Fig. 10. At a low loading of 0.2 wt%, the CO_2 permeance sharply increases to ~455 GPU in the case of 0.2 wt% GO and to 610 GPU in the case of 0.2 wt% pGO. It is believed that both GO and pGO effectively disrupt polymer chain packing while simultaneously increasing CO_2 sorption and reorienting water distribution in the matrix. The difference in permeance between the fillers is attributed to the presence of non-selective pores in pGO when compared to GO, which reduces diffusional resistance to gas permeation. The selectivity of the hybrid membranes containing both GO and pGO at 0.2 wt% loading rapidly decreases to ~34. The change in the performances can be attributed to the enhanced gas diffusion through the more open, water-swollen matrix altered by the presence of GO, whilst the diffusion of N_2 is more competitive than CO_2. Nevertheless, at low GO loadings, these 2D fillers are still too few to cause pronounced diffusional resistance relative to each gas. Similar trends are observed in the pure gas permeation tests albeit with lower CO_2 permeance and selectivity for all cases. The difference is attributed to higher feed partial pressure of CO_2,

which leads to carrier saturation phenomenon in facilitated transport membranes as observed earlier by Wang et al. [24].

Contrary to the expectations, the enhanced compatibility between the GO/SHPAA interface through grafted hydrophilic PEG groups onto the GO surface did not bring in improvement in CO_2 permeation, but resulted in a lower CO_2 permeance in the hybrid membranes compared with membranes containing other GO fillers at 0.2 wt% loading, as seen in Fig. 11. This performance behaviour features as a typical class of hybrid membranes with rigidified interface between nanofillers and the polymer matrix, which usually show constant or increased selectivity but decreased gas permeation, as suggested by several researchers [22, 56,57]. In the GO-PEG hybrid membranes, due to the strong interactions between –OH groups on the GO surface and the amine-containing polymeric matrix, there may exist a more occupied space around the GO with interconnected chains formed between the GO surface and the adjacent polymeric matrix. These chains may result in more rigidified interfaces of GO fillers, which, in conjugation with the GO barrier property, may lead to an increase in the CO_2/N_2 selectivity by effective blocking the gas diffusion (both CO_2 and N_2) but effecting little on the CO_2 sorption. On the other hand, the decrease of CO_2 permeance maybe explained by two competing effects of the fillers; with increasing GO-PEG loading, the presence of more GO nanosheets with rigidified interfaces hinders CO_2 diffusion, while more PEG groups on the GO-polymer interface enhances CO_2 sorption. Hence, at 0.5 wt% loading, there is a marginal increase of CO_2 permeance due to enhanced sorption, followed by a decrease at 1.0 wt% loading due to reduced diffusion. Consequently, the CO_2/N_2 separation factor sharply rose to ~90 while reducing the CO_2 permeance down to 205 GPU at a high loading of 1 wt% filler. A similar effect was seen with higher loading of

Fig. 11. Mixed gas permeation performance of hybrid SHPAA/PVA-membranes with GO-based fillers as a function of filler loading measured at 35 °C.
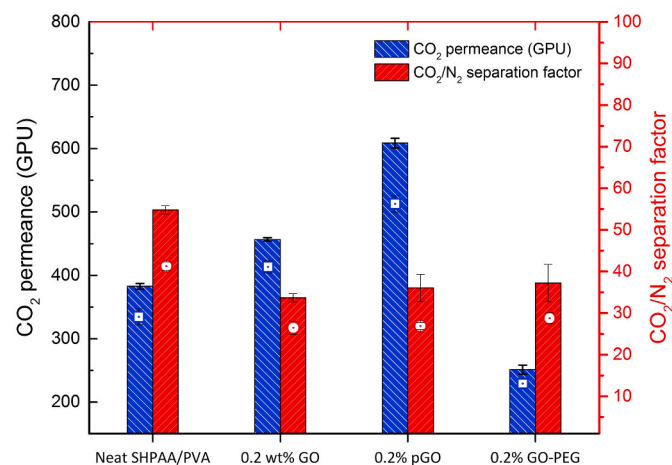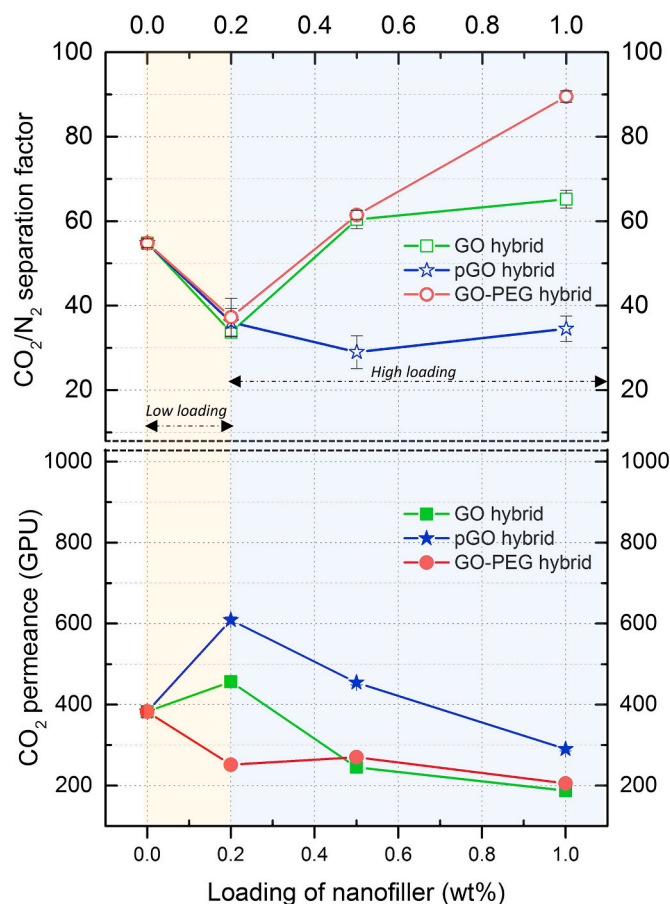
Fig. 10. Mixed gas permeation performance of various SHPAA/PVA-based composite facilitated transport membranes measured at 35 °C. (Symbols denote corresponding pure gas permeation data).

GO nanoplatelets, where the tortuous pathways for N_2 permeation due to the multi-layer orientation of GO leads to increased CO_2/N_2 separation factor of about 65 at 1 wt% loading. Thus, the optimal loading of GO-based fillers for enhanced permeation was observed at 0.2 wt%, above which the effect of barrier property of GO and hence the tortuosity to gas permeation is simultaneously manifested. At this loading, the enhanced permeation of CO_2 due to the polymer chain disruption and increased sorption brought about by the high aspect ratio nanoplatelets counteracts with the resistance caused by the additional tortuosity of the impermeable platelets. At higher loading, the latter effect is found to dominate for both GO and GO-PEG, as seen from the trends in Fig. 11. In the case of pGO, the presence of non-selective pores reduces the tortuosity, but the presence of bulk distribution of small-sized impermeable platelets is still significant. Hence, there is a decline in CO_2 permeance with increasing filler loading, although not as steep as in the case of GO or GO-PEG.

Both the neat SHPAA/PVA membrane and the high permeance SHPAA/PVA-membrane with 0.2 wt% pGO were stored at room temperature under ambient conditions for a period of about 1.5 years and re-tested in humid mixed gas permeation to study the effect of 2D nanofillers in long-term stability of the membrane. It can be seen from Fig. 12 that the neat polymer membrane exhibited reduced permeance of ~25% after 1.5 years when compared to the freshly prepared membranes while increasing the average CO_2/N_2 separation factor from ~55 to ~61. This phenomenon is attributed to relaxation of polymer chains, leading to denser packing and hence reduced diffusivity of permeating species [58]. In facilitated transport membranes, this phenomenon is highly pronounced in the absence of water in the matrix (nearly dry conditions) as the membranes was stored under ambient conditions. The drying of membrane leads to eventual reduction in performance in facilitated transport membranes, typically, reduction in CO_2 flux [13, 59]. Interestingly, even with drying of the membrane, the chain relaxation and densification phenomena were less pronounced in pGO loaded matrix, clearly highlighting the effect of 2D nanoplatelets in redistribution of polymer chain packing. In the latter case, only a reduction of 12% in CO_2 permeance with respect to the freshly prepared membrane was observed with a marginal increase in CO_2/N_2 separation factor.

Very few studies have demonstrated the successful use of physically modified GO for gas transport membranes. He et al. [60] recently reported a positive effect of adding porous GO along with o-hydroxyazo-hierarchical porous organic polymers to PEBAX 1657 membranes, increasing the CO_2 permeability and CO_2/N_2 ideal selectivity to 232.7 Barrer (from 94 barrer) and 80.7 (from 32.4), respectively, although thick films and pure gas conditions were used in the study. Dong et al.

[61] doubled the CO_2 permeability of modified PEBAX 1657 from 60.5 Barrer to 119.5 barrer and selectivity from 54.7 to 103.9 albeit with thick films and at a high loading of 5 wt% of porous GO.

The fabricated membranes in the current study feature as the successful exploitation of porous GO in membranes by now, leading to high CO_2 permeance of up to 607 GPU and CO_2/N_2 separation factor of about 33.5 at a very small loading of pGO at 0.2 wt%.

4. Conclusions

Thin composite facilitated transport membranes with ultrathin selective layer containing 2D nanofillers, i.e., GO, pGO and PEG-GO, were fabricated and tested. By studying different types and loadings of these GO-based 2D nanofillers on the CO_2 separation performance, the effects of 2D nanoplatelets on CO_2 transport properties in the hydrophilic membranes based on PVA matrix and facilitated transport SHPAA/PVA matrix were elucidated. It is speculated that both GO and pGO nanoplatelets positively disrupt polymer chain packing, increase CO_2 sorption, and reorient water distribution in favour of increased CO_2 facilitated transport at a very low loading of 0.2 wt%, while the chemically modified GO-PEG has probably formed a rigidified interface with the amino groups of SHPAA/PVA membrane matrix, leading to increased diffusional resistance and hence lower CO_2 permeance but higher CO_2/N_2 selectivity. Under high PEG-GO loading of 1 wt%, the CO_2/N_2 separation factor increased up to 90 with CO_2 permeance of 205 GPU. The pGO containing SHPAA/PVA membranes at optimal loading exhibited a CO_2 permeance of up to 607 GPU with a CO_2/N_2 separation factor of 36. The high aspect ratio 2D nanosheets induce polymer chain disruption, thereby aiding in retention of permeation performance in membranes for the long-term operation.

The fabricated membranes are identified as the first to successfully demonstrate the potential use of 2D materials in facilitated transport matrices coated in flat sheet configuration with high CO_2 transport properties. As a future work, the positive influence of 2D materials on the polymer chain packing disruption and water channel redistribution at very low loading can be further explored with advanced characterization and molecular studies.

Author contributions

S.J. and L.A. designed the experiments. S.J., J.L.M.E. and X.Y. synthesized the nanofillers and fabricated the membranes, S.J. performed the permeation tests, analysed the results, and wrote the manuscript. L.D. and L.A. conceived the original idea, planned the overall study and
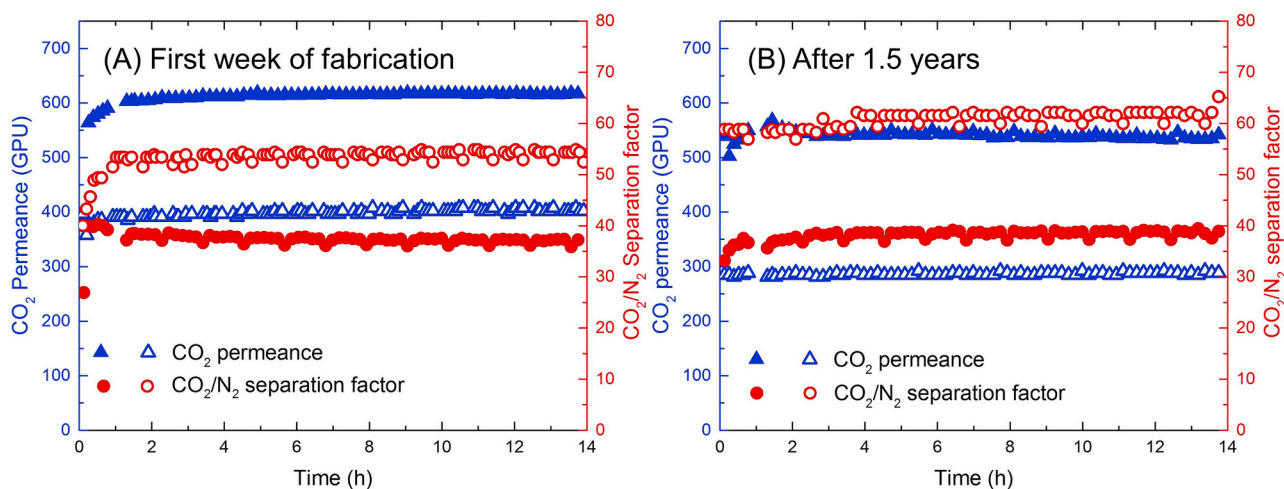

Fig. 12. Mixed gas permeation performance durability of neat SHPAA/PVA-membrane (empty symbols) and SHPAA/PVA-membrane with 0.2 wt% pGO (filled symbols), measured at 35 °C, tested during (A) first week of casting (B) after 1.5 years of storage at room temperature.

supervised the research work.

Author statement

Saravanan Janakiram: Conceptualization, Methodology, Investigation, Writing - original draft, Writing - review & editing. Juan Luis Martín Espejo: Validation, Investigation. Xinyi Yu: Investigation. Luca Ansaloni: Writing - review & editing. Liyuan Deng: Conceptualization, Writing - review & editing, Supervision, Project administration, Funding acquisition.

Declaration of competing interest

The authors declare that they have no known competing financial interests or personal relationships that could have appeared to influence the work reported in this paper.

Acknowledgements

Appendix A. Supplementary data

Supplementary data to this article can be found online at https://doi.org/10.1016/j.memsci.2020.118626.

References

[1] M. Bui, C.S. Adjiman, A. Bardow, E.J. Anthony, A. Boston, S. Brown, P.S. Fennell, S. Fuss, A. Galindo, L.A. Hackett, J.P. Hallett, H.J. Herzog, G. Jackson, J. Kemper, S. Krevor, G.C. Maitland, M. Matuszewski, I.S. Metcalfe, C. Petit, G. Puxty, J. Reimer, D.M. Reiner, E.S. Rubin, S.A. Scott, N. Shah, B. Smit, J.P.M. Trusler, P. Webley, J. Wilcox, N. Mac Dowell, Carbon capture and storage (CCS): the way forward, Energy Environ. Sci. 11 (2018) 1062–1176, https://doi.org/10.1039/c7ee02342a.

[2] I.E.A. (IEA), Energy and climate Change : world energy outlook special report. https://www.iea.org/publications/freepublications/publication/WEO2015SpecialReportonEnergyandClimateChange.pdf, 2015.

[3] M.Z. Jacobson, Review of solutions to global warming, air pollution, and energy security, Energy Environ. Sci. 2 (2008) 148–173, https://doi.org/10.1039/B809990C.

[4] H. Lin, B.D. Freeman, Materials selection guidelines for membranes that remove CO_2 from gas mixtures, J. Mol. Struct. 739 (2005) 57–74, https://doi.org/10.1016/j.molstruc.2004.07.045.

[5] R.D. Noble, Perspectives on mixed matrix membranes, J. Membr. Sci. 378 (2011) 393–397, https://doi.org/10.1016/j.memsci.2011.05.031.

[6] B.D. Freeman, Basis of permeability/selectivity tradeoff relations in polymeric gas separation membranes, Macromolecules 32 (1999) 375–380, https://doi.org/10.1021/ma9814548.

[7] Y. Han, W.S.W. Ho, Recent advances in polymeric membranes for CO_2 capture, Chin. J. Chem. Eng. 26 (2018) 2238–2254, https://doi.org/10.1016/j.cjche.2018.07.010.

[8] L.M. Robeson, The upper bound revisited, J. Membr. Sci. 320 (2008) 390–400, https://doi.org/10.1016/j.memsci.2008.04.030.

[9] H.B. Park, J. Kamcev, L.M. Robeson, M. Elimelech, B.D. Freeman, Maximizing the right stuff: the trade-off between membrane permeability and selectivity, Science 80 (2017) 356, https://doi.org/10.1126/science.aab0530, eaab0530.

[10] S. Janakiram, M. Ahmadi, Z. Dai, L. Ansaloni, L. Deng, Performance of nanocomposite membranes containing 0D to 2D nanofillers for CO_2 separation: a review, Membranes 8 (2018), https://doi.org/10.3390/membranes8020024.

[11] M. Ahmadi, S. Janakiram, Z. Dai, L. Ansaloni, L. Deng, Performance of mixed matrix membranes containing porous two-dimensional (2D) and three-dimensional

(3D) fillers for CO_2 separation: a review, Membranes 8 (2018) 50, https://doi.org/10.3390/membranes8030050.

[12] L. Ansaloni, L. Deng, Advances in Polymer-Inorganic Hybrids as Membrane Materials, Elsevier Ltd, 2016, https://doi.org/10.1016/B978-0-08-100408-1.00007-8.

[13] S. Janakiram, X. Yu, L. Ansaloni, Z. Dai, L. Deng, Manipulation of fibril surfaces in nanocellulose-based facilitated transport membranes for enhanced CO_2 capture, ACS Appl. Mater. Interfaces 11 (2019) 33302–33313, https://doi.org/10.1021/acsami.9b09920.

[14] L. Deng, M.B. Hagg, Carbon nanotube reinforced PVAm/PVA blend FSC nanocomposite membrane for CO_2/CH_4 separation, Int. J. Greenh. Gas Control 26 (2014) 127–134, https://doi.org/10.1016/j.ijggc.2014.04.018.

[15] L. Ansaloni, Y. Zhao, B.T. Jung, K. Ramasubramanian, M.G. Baschetti, W.S.W. Ho, Facilitated transport membranes containing amino-functionalized multi-walled carbon nanotubes for high-pressure CO_2 separations, J. Membr. Sci. 490 (2015) 18–28, https://doi.org/10.1016/j.memsci.2015.03.097.

[16] Z.P. Smith, B.D. Freeman, Graphene oxide: a new platform for high-performance gas- and liquid-separation membranes, Angew. Chem. Int. Ed. 53 (2014) 10286–10288, https://doi.org/10.1002/anie.201404407.

[17] J. Shen, M. Zhang, G. Liu, K. Guan, W. Jin, Size effects of graphene oxide on mixed matrix membranes for CO_2 separation, AIChE J. 62 (2016) 2843–2852, https://doi.org/10.1002/aic.15260.

[18] H.W. Kim, H.W. Yoon, S.-M. Yoon, B.M. Yoo, B.K. Ahn, Y.H. Cho, H.J. Shin, H. Yang, U. Paik, S. Kwon, J.-Y. Choi, H.B. Park, Selective gas transport through few-layered graphene and graphene oxide membranes, Science 80 (342) (2013) 91–95, https://doi.org/10.1126/science.1236098.

[19] G. Dong, Y. Zhang, J. Hou, J. Shen, V. Chen, Graphene oxide nanosheets based novel facilitated transport membranes for efficient CO_2 capture, Ind. Eng. Chem. Res. 55 (2016) 5403–5414, https://doi.org/10.1021/acs.iecr.6b01005.

[20] Y. Shen, H. Wang, J. Liu, Y. Zhang, Enhanced performance of a novel polyvinyl amine/chitosan graphene oxide mixed matrix membrane for CO_2 capture, ACS Sustain. Chem. Eng. 3 (2015) 1819–1829, https://doi.org/10.1021/acssuschemeng.5b00409.

[21] R. Casadei, D. Venturi, M.G. Baschetti, L. Giorgini, E. Maccaferri, S. Ligi, Polyvinylamine membranes containing graphene-based nanofillers for carbon capture applications, Membranes 9 (2019) 119, https://doi.org/10.3390/membranes9090119.

[22] X. Li, Y. Cheng, H. Zhang, S. Wang, Z. Jiang, R. Guo, H. Wu, Efficient CO_2 capture by functionalized graphene oxide nanosheets as fillers to fabricate multi-permselective mixed matrix membranes, ACS Appl. Mater. Interfaces 7 (2015) 5528–5537, https://doi.org/10.1021/acsami.5b00106.

[23] Q. Xin, Z. Li, C. Li, S. Wang, Z. Jiang, H. Wu, Y. Zhang, J. Yang, X. Cao, Enhancing the CO_2 separation performance of composite membranes by the incorporation of amino acid-functionalized graphene oxide, J. Mater. Chem. A. 3 (2015) 6629–6641, https://doi.org/10.1039/C5TA00506J.

[24] Y. Wang, L. Li, X. Zhang, J. Li, C. Liu, N. Li, Z. Xie, Polyvinylamine/graphene oxide/PANI@CNTs mixed matrix composite membranes with enhanced CO_2/N_2 separation performance, J. Membr. Sci. 589 (2019) 117246, https://doi.org/10.1016/j.memsci.2019.117246.

[25] Y. Zhao, W.S.W. Ho, CO_2 - Selective Membranes Containing Sterically Hindered Amines for CO_2/H_2 Separation, vol. 3, 2013, https://doi.org/10.1021/ie301397m.

[26] D.A. Dikin, S. Stankovich, E.J. Zimney, R.D. Piner, G.H.B. Dommett, G. Evmenenko, S.T. Nguyen, R.S. Ruoff, Preparation and characterization of graphene oxide paper, Nature (2007), https://doi.org/10.1038/nature06016.

[27] H. Lee, S.C. Park, J.S. Roh, G.H. Moon, J.E. Shin, Y.S. Kang, H.B. Park, Metal-organic frameworks grown on porous planar template with exceptionally high surface area: promising nanofiller platforms for CO_2 separation, J. Mater. Chem. A. 5 (2017) 22500–22505, https://doi.org/10.1039/C7TA06049A.

[28] Z. Liu, J.T. Robinson, X. Sun, H. Dai, PEGylated nanographene oxide for delivery of water-insoluble cancer drugs, J. Am. Chem. Soc. 130 (2008) 10876–10877, https://doi.org/10.1021/ja803688x.

[29] Z. Dai, J. Deng, L. Ansaloni, S. Janakiram, L. Deng, Thin-film-composite hollow fiber membranes containing amino acid salts as mobile carriers for CO_2 separation, J. Membr. Sci. (2019), https://doi.org/10.1016/j.memsci.2019.02.023.

[30] S. Janakiram, L. Ansaloni, S.-A. Jin, X. Yu, Z. Dai, R.J. Spontak, L. Deng, Humidity-responsive molecular gate-opening mechanism for gas separation in ultraselective nanocellulose/IL hybrid membranes, Green Chem. 22 (2020) 3546–3557, https://doi.org/10.1039/D0GC00544D.

[31] J.F. Moulder, W.F. Stickle, P.E. Sobol, K.D. Bomben, Handbook of X-Ray Photoelectron Spectroscopy: a Reference Book of Standard Spectra for Identification and Interpretation of XPS Data, 1992, 9780962702624.

[32] S. Park, K.S. Lee, G. Bozoklu, W. Cai, S.B.T. Nguyen, R.S. Ruoff, Graphene oxide papers modified by divalent ions - enhancing mechanical properties via chemical cross-linking, ACS Nano 2 (2008) 572–578, https://doi.org/10.1021/nn700349a.

[33] K. Krishnamoorthy, M. Veerapandian, K. Yun, S.J. Kim, The chemical and structural analysis of graphene oxide with different degrees of oxidation, Carbon N. Y. 53 (2013) 38–49, https://doi.org/10.1016/j.carbon.2012.10.013.

[34] Y. Wang, Y. Shao, D.W. Matson, J. Li, Y. Lin, Nitrogen-doped graphene and its application in electrochemical biosensing, ACS Nano 4 (2010) 1790–1798, https://doi.org/10.1021/nn100315s.

[35] J. Liu, H. Yang, S.G. Zhen, C.K. Poh, A. Chaurasia, J. Luo, X. Wu, E.K.L. Yeow, N. G. Sahoo, J. Lin, Z. Shen, A green approach to the synthesis of high-quality graphene oxide flakes via electrochemical exfoliation of pencil core, RSC Adv. 3 (2013) 11745–11750, https://doi.org/10.1039/c3ra41366g.

[36] V. Palermo, I.A. Kinloch, S. Ligi, N.M. Pugno, Nanoscale mechanics of graphene and graphene oxide in composites: a scientific and technological perspective, Adv. Mater. 28 (2016) 6232–6238, https://doi.org/10.1002/adma.201505469.

[37] S. Rapino, E. Treossi, V. Palermo, M. Marcaccio, F. Paolucci, F. Zerbetto, Playing peekaboo with graphene oxide: a scanning electrochemical microscopy investigation, Chem. Commun. 50 (2014) 13117–13120, https://doi.org/10.1039/c4cc06368f.

[38] L. Chen, Z. Xu, J. Li, B. Zhou, M. Shan, Y. Li, L. Liu, B. Li, J. Niu, Modifying graphite oxide nanostructures in various media by high-energy irradiation, RSC Adv. 4 (2014) 1025–1031, https://doi.org/10.1039/c3ra46203j.

[39] H. Zhang, D. Hines, D.L. Akins, Synthesis of a nanocomposite composed of reduced graphene oxide and gold nanoparticles, Dalton Trans. 43 (2014) 2670–2675, https://doi.org/10.1039/c3dt52573b.

[40] H. Bai, W. Jiang, G.P. Kotchey, W.A. Saidi, B.J. Bythell, J.M. Jarvis, A.G. Marshall, R.A.S. Robinson, A. Star, Insight into the mechanism of graphene oxide degradation via the photo-fenton reaction, J. Phys. Chem. C 118 (2014) 10519–10529, https://doi.org/10.1021/jp503413s.

[41] A. Lak, J. Dieckhoff, F. Ludwig, J.M. Scholtyssek, O. Goldmann, H. Lünsdorf, D. Eberbeck, A. Kornowski, M. Kraken, F.J. Litterst, K. Fiege, P. Mischnick, M. Schilling, Highly stable monodisperse PEGylated iron oxide nanoparticle aqueous suspensions: a nontoxic tracer for homogeneous magnetic bioassays, Nanoscale 5 (2013) 11447–11455, https://doi.org/10.1039/c3nr02197a.

[42] S. Park, D.A. Dikin, S.T. Nguyen, R.S. Ruoff, Graphene oxide sheets chemically cross-linked by polyallylamine, J. Phys. Chem. C 113 (2009) 15801–15804, https://doi.org/10.1021/jp907613s.

[43] Y. Zhang, Q. Shen, J. Hou, P.D. Sutrisna, V. Chen, Shear-aligned graphene oxide laminate/Pebax ultrathin composite hollow fiber membranes using a facile dip-coating approach, J. Mater. Chem. A. 5 (2017) 7732–7737, https://doi.org/10.1039/c6ta10395b.

[44] S.J. Lue, Y.L. Pai, C.M. Shih, M.C. Wu, S.M. Lai, Novel bilayer well-aligned Nafion/graphene oxide composite membranes prepared using spin coating method for direct liquid fuel cells, J. Membr. Sci. 493 (2015) 212–223, https://doi.org/10.1016/j.memsci.2015.07.007.

[45] Y. Li, Z. Yang, H. Qiu, Y. Dai, Q. Zheng, J. Li, J. Yang, Self-aligned graphene as anticorrosive barrier in waterborne polyurethane composite coatings, J. Mater. Chem. A. 2 (2014) 14139–14145, https://doi.org/10.1039/c4ta02262a.

[46] V. Berry, Impermeability of graphene and its applications, Carbon N. Y. 62 (2013) 1–10, https://doi.org/10.1016/j.carbon.2013.05.052.

[47] D. Zhan, Z. Ni, W. Chen, L. Sun, Z. Luo, L. Lai, T. Yu, A. Thye, S. Wee, Z. Shen, Electronic structure of graphite oxide and thermally reduced graphite oxide, Carbon N. Y. 49 (2010) 1362–1366, https://doi.org/10.1016/j.carbon.2010.12.002.

[48] O.C. Compton, S. Kim, C. Pierre, J.M. Torkelson, S.T. Nguyen, Crumpled graphene nanosheets as highly effective barrier property enhancers, Adv. Mater. 22 (2010) 4759–4763, https://doi.org/10.1002/adma.201000960.

[49] S. Ben Hamouda, Q.T. Nguyen, D. Langevin, S. Roudesli, Poly(vinylalcohol)/poly (ethyleneglycol)/poly(ethyleneimine) blend membranes - structure and CO_2 facilitated transport, Compt. Rendus Chem. 13 (2010) 372–379, https://doi.org/10.1016/j.crci.2009.10.009.

[50] L. Deng, T.J. Kim, M.B. Hägg, Facilitated transport of CO_2 in novel PVAm/PVA blend membrane, J. Membr. Sci. 340 (2009) 154–163, https://doi.org/10.1016/j.memsci.2009.05.019.

[51] J. Huang, J. Zou, W.S.W. Ho, Carbon dioxide capture using a CO_2-selective facilitated transport membrane, Ind. Eng. Chem. Res. 47 (2008) 1261–1267, https://doi.org/10.1021/ie070794r.

[52] D. Peng, S. Wang, Z. Tian, X. Wu, Y. Wu, H. Wu, Q. Xin, J. Chen, X. Cao, Z. Jiang, Facilitated transport membranes by incorporating graphene nanosheets with high zinc ion loading for enhanced CO_2 separation, J. Membr. Sci. 522 (2017) 351–362, https://doi.org/10.1016/j.memsci.2016.09.040.

[53] R.K. Joshi, S. Alwarappan, M. Yoshimura, V. Sahajwalla, Y. Nishina, Graphene oxide: the new membrane material, Appl. Mater. Today. 1 (2015) 1–12, https://doi.org/10.1016/j.apmt.2015.06.002.

[54] Q. Xin, Y. Gao, X. Wu, C. Li, T. Liu, Y. Shi, Y. Li, Z. Jiang, H. Wu, X. Cao, Incorporating one-dimensional aminated titania nanotubes into sulfonated poly (ether ether ketone) membrane to construct CO_2-facilitated transport pathways for enhanced CO_2 separation, J. Membr. Sci. 488 (2015) 13–29, https://doi.org/10.1016/j.memsci.2015.02.047.

[55] S. Zhao, Z. Wang, Z. Qiao, X. Wei, C. Zhang, J. Wang, S. Wang, Gas separation membrane with CO_2-facilitated transport highway constructed from amino carrier containing nanorods and macromolecules, J. Mater. Chem. A. 1 (2013) 246–249, https://doi.org/10.1039/C2TA00247G.

[56] T.S. Chung, L.Y. Jiang, Y. Li, S. Kulprathipanja, Mixed matrix membranes (MMMs) comprising organic polymers with dispersed inorganic fillers for gas separation, Prog. Polym. Sci. 32 (2007) 483–507, https://doi.org/10.1016/j.progpolymsci.2007.01.008.

[57] L. Ansaloni, L. Deng, Advances in Polymer-Inorganic Hybrids as Membrane Materials, 2016, https://doi.org/10.1016/B978-0-08-100408-1.00007-8.

[58] Y. Huang, D.R. Paul, Physical aging of thin glassy polymer films monitored by gas permeability, Polymer (Guildf). 45 (2004) 8377–8393, https://doi.org/10.1016/j.polymer.2004.10.019.

[59] M.B. Hägg, A. Lindbråthen, X. He, S.G. Nodeland, T. Cantero, Pilot demonstration-reporting on CO_2 capture from a cement plant using hollow fiber process, Energy Procedia 114 (2017) 6150–6165, https://doi.org/10.1016/j.egypro.2017.03.1752.

[60] R. He, S. Cong, J. Wang, J. Liu, Y. Zhang, Porous graphene oxide/porous organic polymer hybrid nanosheets functionalized mixed matrix membrane for efficient CO_2 capture, ACS Appl. Mater. Interfaces 11 (2019) 4338–4344, https://doi.org/10.1021/acsami.8b17599.

[61] G. Dong, J. Hou, J. Wang, Y. Zhang, V. Chen, J. Liu, Enhanced CO_2/N_2 separation by porous reduced graphene oxide/Pebax mixed matrix membranes, J. Membr. Sci. 520 (2016) 860–868, https://doi.org/10.1016/j.memsci.2016.08.059.